

Partial order in a frustrated Potts model

Ryo Igarashi^{1,2,*} and Masao Ogata³

¹CCSE, Japan Atomic Energy Agency, Higashi-Ueno, Taito-ku, Tokyo 110-0015, Japan

²CREST(JST), Honcho, Kawaguchi, Saitama 443-0012, Japan

³Department of Physics, University of Tokyo, Hongo, Bunkyo-ku, Tokyo 133-0033, Japan

(Dated: February 13, 2022)

We investigate a 4-state ferromagnetic Potts model with a special type of geometrical frustration on a three dimensional diamond lattice by means of Wang-Landau Monte Carlo simulation motivated by a peculiar structural phase transition found in β -pyrochlore oxide KOs_2O_6 . We find that this model undergoes unconventional first-order phase transition; half of the spins in the system order in a two dimensional hexagonal-sheet-like structure, while the remaining half stay disordered. The ordered sheets and the disordered sheets stack one after another. We obtain a fairly large residual entropy at $T = 0$ which originates from the disordered sheets.

PACS numbers: 75.10.Hk, 05.50.+q, 05.10.Ln, 02.70.Uu

I. INTRODUCTION

Generally speaking, frustrated systems have some constraints that forbid simultaneous minimization of all the interaction energies. Therefore, frustration usually suppresses phase transitions to long-range orders, and, as a result, leads to very rich low temperature phases. Moreover, a frustrated system may become a spin-liquid phase or sometimes exhibit phase transition to a partially ordered state. In this paper, we study a 4-state ferromagnetic Potts model with a special type of geometrical frustration on a three-dimensional diamond lattice. This model is proposed as a simplified model Hamiltonian for a peculiar phase transition found in β -pyrochlore oxide KOs_2O_6 . Although the obtained phase transition in this model does not explain that in KOs_2O_6 , we find that it has several interesting properties as a model with geometrical frustration.

Let us briefly summarize experimental results of β -pyrochlore superconductors, AOs_2O_6 (A is one of K, Rb or Cs)^{1,2,3,4}, from which the particular model studied in this paper is derived. We mainly focus on the anomalous phase transition other than superconducting transition in KOs_2O_6 . The pyrochlore structure in general is of type $\text{A}'_2\text{B}'_2\text{O}_6\text{O}'$ with cubic space-group $Fd\bar{3}m$ ^{5,6}. The four crystallographically inequivalent atoms A', B', O, and O' occupy the $16c$, $16d$, $48f$, and $8b$ sites, respectively, in the fcc unit cell. The crystal structure of the β -pyrochlore is derived from the general pyrochlore structure by removing A' atoms, by replacing O' (oxygen) atoms with alkali metal atoms, and by filling the B' position with osmium atoms. The superconducting transition temperature, T_c , of this β -pyrochlore oxide family is rather high^{2,3,4,7,8} compared with the previously discovered pyrochlore oxide superconductor, $\text{Cd}_2\text{Re}_2\text{O}_7$ ⁹.

Several first-principle density functional calculations were performed for the various β -pyrochlore compounds^{10,11}. The electric structure is not affected by changing the alkali atoms which are almost univalent. The osmium atoms and the oxygen atoms form OsO_6 octahedra and OsO_6 network acts as cages for the alkali

atoms. The cage size is also insensitive to the alkali atom content^{2,5}. Therefore, the difference of T_c among the β -pyrochlore family comes from the size mismatch between the cages and the alkali atoms. The heaviest anharmonic oscillation called “rattling” is observed for the smallest alkali atom contents, K^{5,11,12}. The spatial asymmetry of the electron density of K atoms is also observed^{5,13}, which favors the nearest neighbor K atom direction.

Aside from the superconductivity, the potassium based β -pyrochlore KOs_2O_6 undergoes a novel phase transition near 7.6K ^{1,14,15}. This is a first-order phase transition where both specific heat and resistivity show hysteresis^{16,17}. Surprisingly, its transition temperature is independent of the superconducting T_c . Therefore, this transition is not an electric origin and is assumed to be of structural one which relates to the “rattling” of the K atoms. However, no evidence for lattice distortion has been found in X-ray, NMR^{18,19}, high pressure transport measurements²⁰, scanning tunneling spectroscopy²¹, the photo-emission spectroscopy²² or Raman spectroscopy^{23,24,25} measurements. Thus, in spite of the very sharp transition, the nature of the phase transition remains a big mystery.

II. MODEL

Having the peculiar first-order phase transition of KOs_2O_6 described above in mind, we study a simple classical model with special kind of geometrical frustration, which was proposed by Kunès *et al.* using the density functional calculation^{11,26,27,28}. They investigated that the on-site potential of the K atoms along with K-K bond direction is heavily unharmonic and very flat near the symmetry center, which is formed by osmium and oxygen surrounding the K ion is over-sized.

The cages formed by OsO_6 octahedra in the β -pyrochlore structure have 4 holes towards nearest-neighbor K atoms because the $16c$ sites are empty. Therefore these four holes in the cages are not only the origin of anisotropic potential of a K atom but also the origin

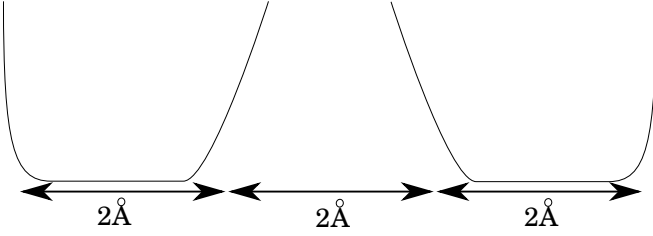


FIG. 1: An approximate length-scale image of the potential wells for K atoms. The bond center is the inversion symmetry center.

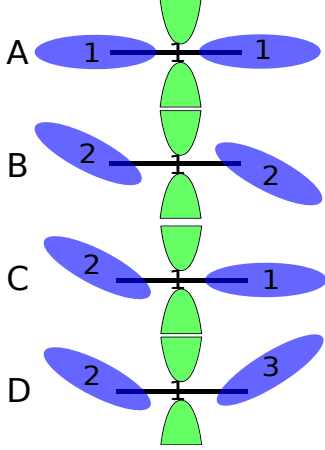


FIG. 2: (Color Online) Some examples of configurations of “bond number”, $R(ij)$, and Potts variable α at both ends. Each oval means that one of the four wavefunctions, $\alpha = 1, 2, 3, 4$, extending in some direction. The green structures represent that the Os-O cage have holes towards the next-nearest K atoms. Configuration A: two wavefunctions and the bond are all parallel. This gives an energy of $-2J_1 + 2J_2$ and is energetically unfavored since $J_2 > J_1$. Configuration B: two wavefunctions are parallel but the bond direction is different case. This gives an energy of $-2J_1$ and is energetically favored. Configuration C: one of the spins and the bond are parallel but the other spins is not. This gives an energy of J_3 . Configuration D gives an energy of 0.

of rather strong Coulomb interaction between K atoms. The K atoms in the β -pyrochlore KOs_2O_6 form the diamond lattice structure. Thus the coupling between the nearest-neighbor K atoms is essentially of Coulomb origin and repulsive. Actually, as shown in the approximate length scale of the cage and the flat potential region of the K atoms in Fig. 1, the distance between cages is very small.

For discussing K atoms quantum mechanically, it is useful to use the states $|\alpha\rangle$ ($\alpha = 1, 2, 3, 4$) as the basis which represents the sp^3 -like wavefunctions made out of $1s$ and $2p$ states, each located towards the holes of the cages. The cages will play the roll of metallic screening and thus we assume that the further long-range interaction can be neglected. The flat potential and the

holes in cages lessen the energy difference between the singlet and triplet states and increases the energy difference to the higher energy states. Therefore we focus on the lowest four states and neglect the energy difference between the lowest singlet and triplet states. In this case we can assume the four-fold degenerate basis states, $|\alpha\rangle$ ($\alpha = 1, 2, 3, 4$), for each K atom in every cage. These states can be represented in the sp^3 -like structure which point to the nearest-neighbor K atoms. We assign these states as the four states of the classical Potts model. Note that we have one-to-one correspondence between the Potts variable 1 to 4 and the direction in the diamond lattice.

We concentrate on the inter-site Coulomb couplings represented in the lowest 4 states. Although there are 4^4 matrix elements, $\langle\alpha\beta|W|\alpha'\beta'\rangle$, the largest contribution comes from the diagonal matrix elements, $\langle\alpha\beta|W|\alpha\beta\rangle$ ^{26,27,28}. These matrix elements are estimated to be

$$\begin{aligned} \langle\alpha\beta|W_R|\alpha\beta\rangle &= -2J_1\delta_{\alpha\beta} + 2J_2\delta_{\alpha R}\delta_{\beta R} - J_3(\delta_{\alpha R} + \delta_{\beta R}) \\ &\quad (J_1 = 162\text{K}, J_2 = 371\text{K}, J_3 = 301\text{K}) \end{aligned} \quad (1)$$

where α and β denotes the direction of the bond, $\delta_{\alpha\beta}$ is the Kronecker delta and R is a so-called “bond number”, which represents the 4 type of bond directions in the diamond lattice structure and takes the value of 1 to 4. For example, $R = 1$ means that the direction of the bond is $\langle 111 \rangle$, and similarly the basis state with $\alpha = 1$ represents one of the four wavefunctions extending in the $\langle 111 \rangle$ direction. 4 types of typical configurations are shown in Fig. 2. The first term in the right-hand-side of eq. (1) represents the energy gain of $2J_1$ when K atoms on the both ends of a bond are in the same direction $\alpha = \beta$. For example, the configuration A and B in Fig. 2 corresponds to this case. The second term in the right-hand-side of eq. (1) means that there is an energy loss of $2J_2$ when the bond direction (R) and the directions of the states $|\alpha\rangle$ and $|\beta\rangle$ at the both ends of the bonds are all in a straight line. The configuration A in Fig. 2 also corresponds to this case. The third term in the right-hand-side of eq. (1) represents the energy gain of J_3 when the wavefunction of one side is parallel to the bond direction. This corresponds to the configuration C in Fig. 2. As a result, configuration A in Fig. 2 has an energy, $-2J_1 + 2J_2$, configuration B, $-2J_1$, configuration C, $-J_3$ and configuration D, zero. We can neglect the J_3 terms because these terms corresponds to the constant value after summation of all bonds.

The off-diagonal terms, such as $\langle\alpha\beta|W|\alpha\gamma\rangle$, is of order smaller than J_1 , J_2 and J_3 . Therefore we neglect the off-diagonalized terms in the following. Furthermore, we assume that the effects of the excited states higher than the lowest four states are negligible. Finally, the effective Hamiltonian for the inter-site couplings of K atoms

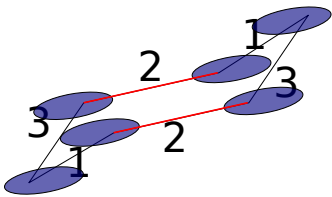


FIG. 3: (Color Online) Illustration of the geometrical frustration introduced in this model is shown. The first closed loop consists of 6 variables and 6 variables ferromagnetically orders to “2” state. In this situation, the energy loss in the two number “2” bonds. there are no energy loss when we assign “4” state to this loop but there are direction of the loop that “4” state have energy loss.

becomes

$$H = \sum_{\langle ij \rangle} \left(-J_1 \delta_{\alpha\beta}^{ij} + J_2 \delta_{\alpha R(ij)}^i \delta_{\beta R(ij)}^j \right), \quad (2)$$

where $R(ij)$ is also a so-called “bond number”, 1–4, between i -site and j -site, which takes the same value of R described above. J_1 term shows energy gain of parallel oscillation of K ion and J_2 term shows energy loss of oscillation in line. The bare values of J_1 and J_2 are 162K and 371K, respectively²⁷. The sum is taken over the K–K bond network forming the diamond lattice structure.

When $J_2 = 0$, this Hamiltonian describes the classical ferromagnetic 4-state Potts model on the diamond lattice. The second term gives a peculiar interaction and the origin of frustration as shown in Fig. 3. If we consider a ferromagnetic state, *i.e.*, a state where all the K atoms are in the same wavefunction $|\alpha\rangle$, there must be always several bonds where the two wavefunctions at the both ends are parallel to the bond direction (Number 2 bond in Fig. 3). This gives a frustration. Note that the term “the frustration in the pyrochlore lattice” usually indicates the electric one which comes from the tetragonal-structure network formed by osmium and oxygen atoms. However, the origin of the frustration in KOs_2O_6 described here is completely different. The frustration comes intrinsically from the inter-site coupling between K atoms in the diamond lattice.

III. METHOD

The three dimensional 4-state ferromagnetic Potts model undergoes the first order transition²⁹. In order to handle the possible first order phase transition within the Monte Carlo simulation framework, we choose the Wang-Landau algorithm^{30,31,32,33}. This method enables us to calculate directly the density of states (DOS), $g(E)$, and also allows us to efficiently sample the ground state. This algorithm is very effective for studying first-order phase transitions. The various thermodynamical quantities are also obtained very accurately even near the first-order phase transition temperature. Furthermore, this method

can give estimates of the accurate ground state structure, the ground state energy and residual entropy, all of which are not obtained before.

This algorithm works as follows. Since the density of states, $g(E)$, is *a priori* not known at the very beginning of the simulation, we first simply set $g(E) = 1$ for all possible energies E . Then we continue to update $g(E)$ until it converges to a reasonable functional form and the energy histogram $h(E)$ becomes flat. We construct a Markov chain of microscopic configuration $\{\mu\}$ using the local update scheme. We accept the new configuration using the transition probability

$$p(\mu_1 \rightarrow \mu_2) = \min \left[\frac{g(E_{\mu_1})}{g(E_{\mu_2})}, 1 \right], \quad (3)$$

where E_{μ_1} and E_{μ_2} are the energy of the system in a specific configuration μ_1 and μ_2 , respectively. The calculated density of states $g(E)$ and the energy histogram $h(E)$ are updated regardless of the acceptance of the new configuration as

$$\ln g(E_\mu) \rightarrow \ln g(E_\mu) + \ln f_i \quad (4)$$

$$h(E_\mu) \rightarrow h(E_\mu) + 1, \quad (5)$$

where f_i is a modification factor of the i th step of the Wang-Landau algorithm, as defined below. At first, f_1 is chosen as $f_1 = e$. After some iteration, we then check the “flatness” of the obtained energy histogram $h(E)$ by using a criteria that the minimum value of $h(E)$ is not less than 80% of the average of the histogram, *i.e.*,

$$h(E)|_{\min} \geq 0.8 \times \langle h(E) \rangle. \quad (6)$$

When the “flatness” of the histogram is reached, go to the $(i + 1)$ th step of the Wang-Landau algorithm, by changing the modification factor as

$$\ln f_{i+1} = a \ln f_i, \quad (7)$$

$$(0 < a < 1)$$

where we choose $a = 0.5$, and also reset the energy histogram. We repeat until the $i = 16$ Wang-Landau step. The choice of $i = 16$ and $a = 0.5$ gives a reasonable convergence of $g(E)$ for the 4-state Potts model³⁰.

We carry out the Monte Carlo simulations with different seeds for pseudo random number generator and calculated the average and variance of each quantity for $J_2 = \infty$ and $J_2 = 10$. We use $8^3 = 512$ unit cells, each consists of 8 atoms and therefore the total number is 4096.

IV. RESULTS

Figure 4 shows the results of energy density for the case of $J_2 = \infty$. We can see a clear kink at $T \sim 0.44$ which indicates a first-order phase transition of the model. We also find that the ground state energy density is equal

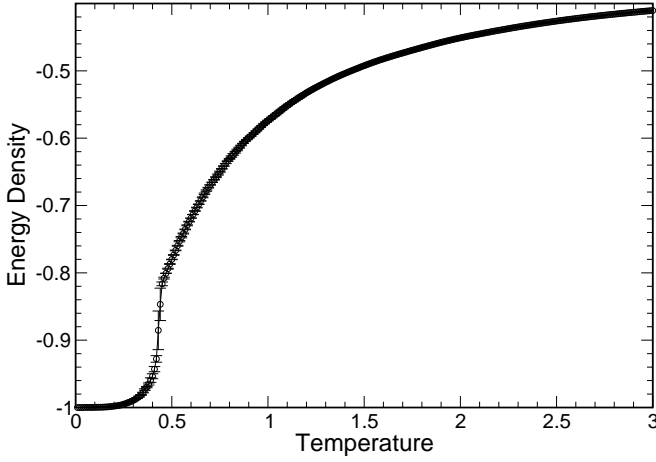


FIG. 4: Energy density calculation of the extended Potts model with $J_2 = \infty$. This results is of 8^3 unit cells and consists of 4096 sites.

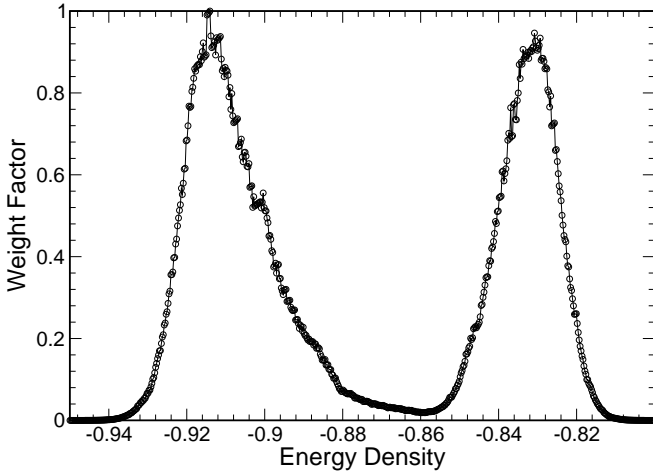


FIG. 5: Weight factor $g(E)\exp(-\beta E)$ as a function of the energy density E , in the case of $J_2 = 10$ near the transition temperature. This results is of 8^3 unit cells and consists of 4096 sites.

to -1 per site within the statistical error. If $J_2 = 0$, the ground state energy density should be exactly -2 , because the model is reduced to the ordinary 4-state ferromagnetic Potts model with $2N$ bonds in the diamond lattice. This result indicates that the ground state of the present model is different from the simple ferromagnetic ground state due to the frustration induced by J_2 term.

In order to confirm the first-order phase transition, we study the weight factor, $g(E)\exp(-\beta E)$, as a function of the energy density E . Figure 5 shows the obtained weight factor of $J_2 = 10$ and $T = 0.435$ case. The double-peak structure is a clear evidence of the first-order phase transition. We confirmed that this double-peak structure disappears when the temperature is only slightly off the transition temperature, for example, at $T = 0.45$ or $T = 0.42$.

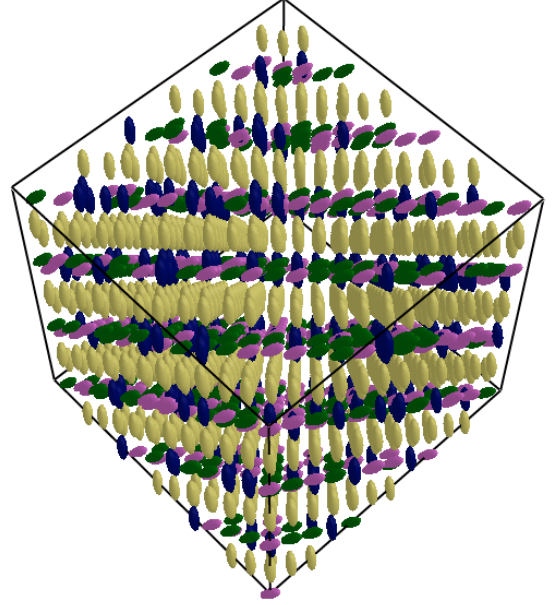


FIG. 6: (Color Online) Snapshot of the ground state of $6 \times 6 \times 6$ lattice (1728 atoms). The pole direction of the ellipsoid indicate the orientation of wavefunction represented by a Potts variable..

A snapshot of the ground state is shown in Fig. 6. We can see that half of the wavefunctions $|\alpha\rangle$ represented by Potts variables order in a two-dimensional hexagonal sheet-like structure, in which half sites are located slightly above the sheet and the remaining half slightly below. This sheet-like plane is perpendicular to the majority rattling direction. The sandwiched sheets between the directions of the majority wavefunction remain disordered consisting of the other three wavefunctions. This ground state structure is a very new and peculiar ground state structure induced by an interesting frustration interaction in the present model.

Let us now discuss the residual entropy density originating from the disordered sheets. The obtained entropy density as a function of T in the case with $J_2 = 10$ is shown in Fig. 7. We find that the entropy density in the $T \rightarrow \infty$ limit converges to $1.092(6)$ when we set the ground-state entropy to be zero. The correct entropy density in the $T \rightarrow \infty$ limit should become

$$\langle S \rangle (T \rightarrow \infty) = \log 4, \quad (8)$$

since every site has 4 degrees of freedom in the present model. Therefore the residual entropy density in the present model is calculated as

$$\langle S_0 \rangle = \log 4 - 1.092 = 0.294. \quad (9)$$

This residual entropy density must come from the degenerate ground state of the disordered sheets as shown in Fig. 8.

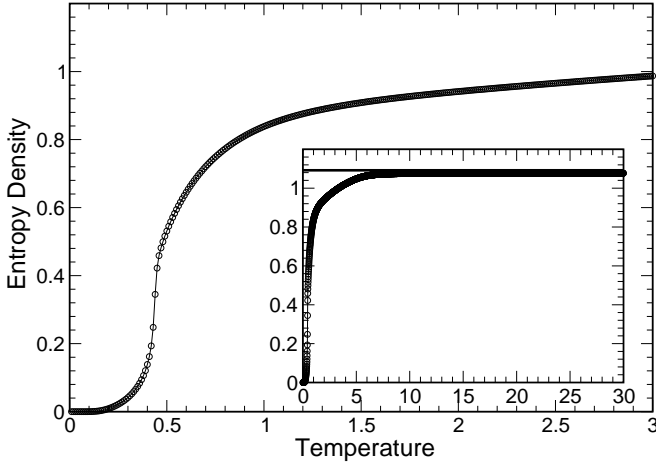


FIG. 7: Entropy density calculations of the extended Potts model with $J_2 = 10$ are shown. These results are of 8^3 unit cells and consists of 4096 sites and the calculation up to the temperature $T = 3$ is shown. The jump of the Entropy density is observed at $T \sim 0.44$ which corresponds to the first order phase transition temperature. The inset shows the calculation up to the temperature $T = 30$. The line denotes the value of 1.092.

In the following, we consider the residual entropy in detail. Two examples of the ground state configurations are shown in Fig. 8. Here the bonds with “bond number” 4 are perpendicular to the hexagonal sheet, and it is assumed that all the sites in the nearest-neighbor sheet have Potts variable 4. Therefore, the Potts variable 4 is forbidden in the sheets shown in Fig. 8. Therefore, if the Potts variables in the disordered sheets with $N/2$ sites are completely random, the total number of possible configurations is $3^{N/2}$ and the corresponding entropy density is

$$\langle S'_0 \rangle = \frac{1}{N} \log 3^{N/2} = 0.5493. \quad (10)$$

However, the residual entropy density in eq. (9) is much smaller than that calculated in eq. (10). The origin of this difference comes from the constraint inside the disordered sheet.

Actually, a bond direction and the two states at the both ends of the bond cannot be all parallel inside the disordered sheet. Even under the constraint, there are many possible configurations in the ground state. The upper figure and the lower figure of Fig. 8 look very different but they have exactly the same energy. The upper figure has a site-number unbalance. The $\frac{N}{4}$ sites are filled with Potts variable 1 whereas only $\frac{N}{8}$ sites are filled with Potts variable 2 and 3. In the lower figure, the sites are almost equally filled with the Potts variables 1, 2 and 3. Note that the number of the spins in the sheet shown in Fig. 8 is not dividable by 3 but there is no difficulty of filling Potts variables almost equally.

The effect of the constraint inside the sheets can be

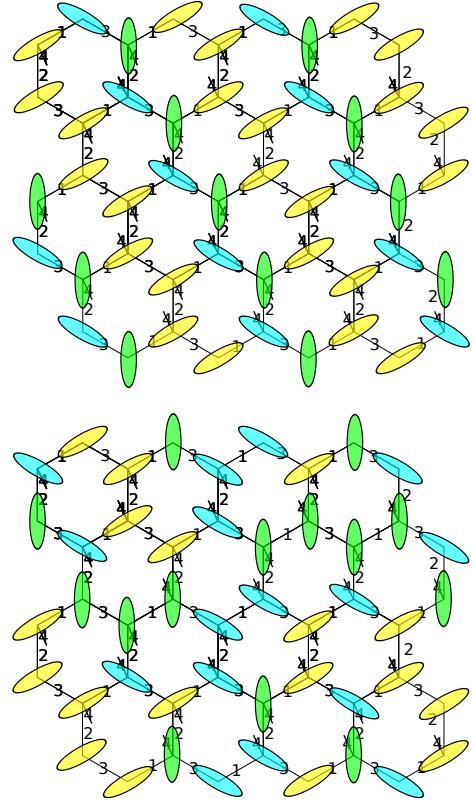


FIG. 8: (Color Online) Two examples of the ground state configurations in a disordered sheet are shown. Both configurations satisfy periodic boundary condition. The yellow, green and blue ellipse denote Potts variable 1, 2 and 3, respectively.

taken into account approximately as follows³⁴: Let us start from the completely random configurations which consists of $3^{N/2}$ states. If we focus on a single bond in the hexagonal sheet, we notice that the forbidden states for that bond are included. Since the configurations are chosen completely randomly, the probability of appearance of this forbidden state is $\frac{1}{9}$. Here $3 \times 3 = 9$ represents the total number of the states at the both ends of the corresponding bond. Therefore, for each bond, $\frac{1}{9}$ configurations should be discarded. As a result, the total number of the allowed configurations can be estimated as

$$3^{N/2} \left(1 - \frac{1}{9}\right)^{\frac{3}{4}N} = \frac{8^{3/4}N}{3^N}, \quad (11)$$

where $\frac{3}{4}N$ is the number of bonds in the sheet. The resulting entropy density is given by

$$S_0 = \log \left(\frac{8^{3/4}}{3} \right) = \log(1.586) = 0.461, \quad (12)$$

which is closer to the numerically obtained residual entropy density, 0.294, than the completely random value 0.5493.

V. DISCUSSION AND CONCLUSIONS

Let us compare the present results with experiments of KOs_2O_6 . Despite the various peculiar properties of the present model, it apparently shows directional symmetry breaking, which is not observed in KOs_2O_6 . The transition temperature of the model, $0.44J_1 \sim 80\text{K}$, is of order high compared with the experimentally obtained first order transition temperature of $T_p = 7.5\text{K}$. Thus, the simplified model proposed by Kuněš *et al.* does not explain the rattling transition in KOs_2O_6 . A more sophisticated model Hamiltonian will be necessary. Recently, Hattori and Tsunetsugu³⁵ proposed another model for this rattling transition of KOs_2O_6 . They argued the rattling transition by introducing a fifth state in addition to the four states discussed above. Although they succeeded to explain the first-order phase transition without symmetry breaking, the physical origin of the fifth state is not clear. Moreover, a recent experiments shows that the lattice expands below T_p , which contradicts their prediction. Thus the rattling transition in KOs_2O_6 remains an open question.

Although the present model is not applied to the transition in KOs_2O_6 , we found that this model has very peculiar features. The obtained phase transition is of first order, which is verified from the double peak structure

of the weight factor shown in Fig. 5. The ground state spin configuration of this model shows that half of the spins in the system are ordered and form a hexagonal-sheet-like structure. The overall possible structures of the ground state snapshot configuration are illustrated in Fig. 6 and Fig. 8. The remaining half of the spins are distributed disordered even in the low temperature limit $T \rightarrow 0$, which gives the residual entropy density of $0.294(6)$. These results indicate a new kind of interesting ground state which will be worth further studying as a result of new type of frustration. We use the ALPS library for calculation³⁶.

Acknowledgments

We are grateful to Dr. Todo (Department of Applied Physics, University of Tokyo) for allowing to use the part of the ALPS parapak library. This work is supported in part by Global COE Program “the Physical Sciences Frontier”, MEXT, Japan. The computation in this work has in part been done using the facilities of the Supercomputer Center, Institute for Solid State Physics, University of Tokyo and the Next Generation Super Computing Project, Nanoscience Program, MEXT, Japan.

-
- * Electronic address: igarashi.ryo@jaea.go.jp
- ¹ Z. Hiroi, S. Yonezawa, J. Yamaura, T. Muramatsu, and Y. Muraoka, J. Phys. Soc. Jpn. **74**, 1682 (2005), erratum at J. Phys. Soc. Jpn. **74**, 3400.
 - ² S. Yonezawa, Y. Muraoka, Y. Matsushita, and Z. Hiroi, J. Phys. Soc. Jpn. **73**, 819 (2004), erratum at J. Phys. Soc. Jpn. **74**, 3400.
 - ³ S. Yonezawa, Y. Muraoka, and Z. Hiroi, J. Phys. Soc. Jpn. **73**, 1655 (2004).
 - ⁴ S. Yonezawa, Y. Muraoka, Y. Matsushita, and Z. Hiroi, J. Phys.: Condens. Matter **16**, L9 (2004).
 - ⁵ J. Yamaura, S. Yonezawa, Y. Muraoka, and Z. Hiroi, J. Solid State Chem. **179**, 336 (2006).
 - ⁶ G. Chuck, S. M. Kazakov, K. Rogacki, N. D. Zhigadlo, and J. Karpinski, Phys. Rev. B **73**, 144506 (2006).
 - ⁷ S. M. Kazakov, N. D. Zhigadlo, M. Brühwiler, B. Batlogg, and J. Karpinski, Supercond. Sci. Technol. **17**, 1169 (2004).
 - ⁸ M. Brühwiler, S. M. Kazakov, N. D. Zhigadlo, J. Karpinski, and B. Batlogg, Phys. Rev. B **70**, 020503(R) (2004).
 - ⁹ M. Hanawa, Y. Muraoka, T. Tayama, T. Sakakibara, J. Yamaura, and Z. Hiroi, Phys. Rev. Lett. **87**, 187001 (2001).
 - ¹⁰ R. Saniz, J. E. Medvedeva, L.-H. Ye, T. Shishidou, and A. J. Freeman, Phys. Rev. B **70**, 100505(R) (2004).
 - ¹¹ J. Kuneš, T. Jeong, and W. E. Pickett, Phys. Rev. B **70**, 174510 (2004).
 - ¹² Z. Hiroi, S. Yonezawa, T. Muramatsu, J. Yamaura, and Y. Muraoka, J. Phys. Soc. Jpn. **74**, 1255 (2005), erratum at J. Phys. Soc. Jpn. **74**, 3400.
 - ¹³ R. Galati, R. W. Hughes, C. S. Knee, P. F. Henry, and M. T. Weller, J. Mater. Chem. **17**, 160 (2007).
 - ¹⁴ Z. Hiroi, S. Yonezawa, J. Yamaura, T. Muramatsu, Y. Matsushita, and Y. Muraoka, J. Phys. Soc. Jpn. **74**, 3400 (2005).
 - ¹⁵ M. Brühwiler, S. M. Kazakov, J. Karpinski, and B. Batlogg, Phys. Rev. B **73**, 094518 (2006).
 - ¹⁶ Z. Hiroi, S. Yonezawa, Y. Nagao, and J. Yamaura, Phys. Rev. B **76**, 014523 (2007).
 - ¹⁷ Z. Hiroi, S. Yonezawa, and J. Yamaura, J. Phys.: Condens. Matter **19**, 5283 (2007).
 - ¹⁸ M. Yoshida, K. Arai, R. Kaido, M. Takigawa, S. Yonezawa, Y. Muraoka, and Z. Hiroi, Phys. Rev. Lett. **98**, 197002 (2007).
 - ¹⁹ M. Yoshida, K. Arai, R. Kaido, M. Takigawa, S. Yonezawa, Y. Muraoka, and Z. Hiroi, J. Magn. Magn. Mater. **310**, 698 (2007).
 - ²⁰ A. Akrap, E. Tutiš, S. M. Kazakov, N. D. Zhigadlo, J. Karpinski, and L. Forró, Phys. Rev. B **75**, 172501 (2007).
 - ²¹ C. Dubois, G. Santi, I. Cuttat, C. Berthod, N. Jenkins, A. P. Petrović, A. A. Manuel, Ø. Fischer, S. M. Kazakov, Z. Bukowski, et al., Phys. Rev. Lett. **101**, 057004 (2008).
 - ²² T. Shimojima, Y. Shibata, K. Ishizaka, T. Kiss, A. Chainani, T. Yokoya, T. Togashi, X.-Y. Wang, C. T. Chen, S. Watanabe, et al., Phys. Rev. Lett. **99**, 117003 (2007).
 - ²³ T. Hasegawa, Y. Takasu, N. Ogita, M. Udagawa, J. Yamaura, Y. Nagao, and Z. Hiroi, J. Phys.: Conference Series **92**, 2124 (2007).
 - ²⁴ T. Hasegawa, Y. Takasu, N. Ogita, M. Udagawa, J. Yamaura, Y. Nagao, and Z. Hiroi, Phys. Rev. B **77**, 064303 (2008).

- ²⁵ J. Schoenes, A.-M. Racu, K. Doll, Z. Bukowski, and J. Karpinski, Phys. Rev. B **77**, 134515 (2008).
- ²⁶ J. Kuneš and W. E. Pickett, Phys. Status Solidi A **203**, 2962 (2006).
- ²⁷ J. Kuneš and W. E. Pickett, Phys. Rev. B **74**, 094302 (2006).
- ²⁸ J. Kuneš and W. E. Pickett, Physica B **378**, 898 (2006).
- ²⁹ F. Y. Wu, Rev. Mod. Phys. **54**, 235 (1982).
- ³⁰ F. Wang and D. P. Landau, Phys. Rev. E **64**, 056101 (pages 16) (2001).
- ³¹ F. Wang and D. P. Landau, Phys. Rev. Lett. **86**, 2050 (2001).
- ³² D. P. Landau and F. Wang, Comp. Phys. Comm. **147**, 674 (2002).
- ³³ D. P. Landau, S.-H. Tsai, and M. Exler, Amer. J. Phys. **72**, 1294 (2004).
- ³⁴ M. Udagawa, M. Ogata, and Z. Hiroi, J. Phys. Soc. Jpn. **71**, 2365 (2002).
- ³⁵ K. Hattori and H. Tsunetsugu, J. Phys. Soc. Jpn. **78**, 013603 (2009).
- ³⁶ A. F. Albuquerque, F. Alet, P. Corboz, P. Dayal, A. Feiguin, S. Fuchs, L. Gamper, E. Gull, S. Gürtler, A. Honecker, et al., (ALPS Collaboration), J. Magn. Magn. Mater. **310**, 1187 (2007).